Thermochimica Acta, 13 (1975) 15–36

KINETICS AND MECHANISM OF THE DEHYDRATION OF γ-FeOOH

RUDOLF GIOVANOLI AND RUDOLF BRÜTSCH
Laboratory of Electron Microscopy, Institute of Inorganic Chemistry, University of Berne, 3 Freiestrasse, CH-3000 Berne 9 (Switzerland)
(Received 24 March 1975)

ABSTRACT

The dehydration of γ-FeOOH to γ-Fe_2O_3 in vacuo has been investigated by thermoanalysis. Results have been checked by electron microscopy and diffraction and by x-ray diffraction. Authors find that formal kinetics are not conclusive. Electron micrographs, however, show directly that random nucleation occurs, producing perfectly oriented but disordered γ-Fe_2O_3 crystals of about 70 Å size. The results can be accomodated with an atomistic model of lattice collapse.

INTRODUCTION

We have set out in a short communication[1], that a comprehensive treatment of a reaction involving solids should not be restricted to formal kinetics but also include morphological, textural and structural investigations. To specify these terms, brief definitions are necessary:

(i) Structure: Lattice of the initial solid and the reaction products, as defined by a space group. Instrument: X-ray and electron diffraction.

(ii) Texture: Grain, aggregation and crystallite sizes; orientation of crystallites in the aggregations; specific surface; lattice defects and disorder. Instrument: X-ray and electron reflection profile analysis; BET surface determination; single crystal electron diffraction; electron microscopy in the dark field using selected reflections.

(iii) Morphology: Direct observation of nucleation and subsequent proceeding reaction; alterations of particle, aggregation and crystallite. Instrument: electron microscope; where suitable polarizing microscope.

It has been emphasized[2] that a thorough study of apparently trivial reactions involving solids is in fact fairly complex. As the specific surface may seem to be an additional disturbing factor, there is a distinct predelection to investigate single crystals, especially when also suitable for X-ray structural work. Diffusion paths, however, become important under these conditions and will as a rule dominate the time law and the mechanism. Suitably small single crystals, preferably of defined shape and size distribution, will thus be the proper substrate to investigate reactions of solids[2].

Authors are aware of only one reaction studied according to the viewpoint outlined above[3]. The present article deals with the results of another reaction. The dehydration of γ-FeOOH and the occurring structural relations have been studied previously[4,5].

EXPERIMENTAL

1. *Preparation of γ-FeOOH*

A detailed description for well crystallized γ-FeOOH has been published earlier[1]. For comparison two more samples, from the department collection, of unknown history, have also been used. They were distinctly less crystalline.

2. *X-ray procedures*

A focusing Guinier–de Wolff camera mark I and FeK_α radiation were used. Crystallite size determination was performed with data from a Philips–Norelco goniometer using Mn filtered FeK_α radiation and α-SiO$_2$ as reference standard. Profiles were measured with a planimeter, and a $K\alpha_1\alpha_2$ doublet correction was applied. The evaluation followed standard procedures[6].

3. *Electron microscopy*

Samples prepared according to current techniques were investigated in a Siemens Elmiskop I, a Hitachi HU-11A, and a Hitachi HU-12A electron microscope. The lattice resolution of 3 Å of the last mentioned instrument proved to be crucial for the quality of the micrographs even when the magnification was below the upper limit. For that reason cooling and tilting stages with substantial loss in resolution were discarded. It could be shown that specimens were stable enough in the electron beam for some considerable time even when they had been quenched in halfway completed reaction. Each crystal investigated was repeatedly checked by selected area electron diffraction to make quite sure that it remained unaltered in the microscope.

4. *Thermobalance*

Unisothermal and isothermal runs were produced on a Mettler thermoanalyzer TA1 in vacuo (appr. 10^{-5} torr) using Pt–Rh (10%) crucibles of diameter up to 16 mm and sample thickness not exceeding a few tenths of mm.

5. *BET measurements*

The specific surface was determined on a Cahn electrobalance type RG using N$_2$ for adsorption.

RESULTS

1. *Starting materials*

The γ-FeOOH samples used are shown as powder patterns and as electron micrographs in Fig. 1. Figure 1f shows a representative electron diffraction of a single crystal of preparation I.

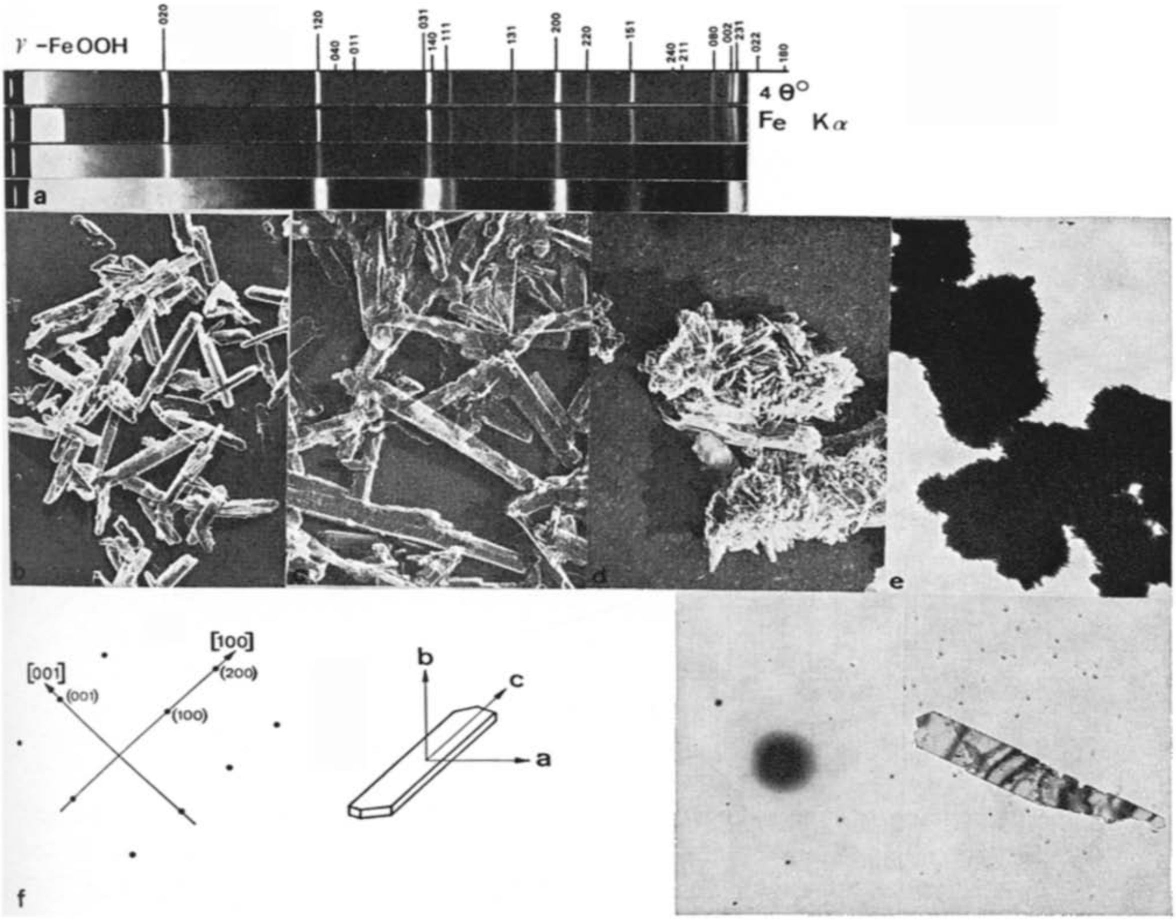

Fig. 1. Starting materials. (a) Guinier patterns of preparations 1–4. (b) Electron micrograph of sample 1 (10'000×). (c) Electron micrograph of sample 2 (20'000×). (d) Electron micrograph of sample 3 (18'000×). (e) Electron micrograph of sample 4 (12'000×). (f) Electron diffraction of a crystal of sample 1 with micrograph of diffracted crystal and indices (20'000×).

TABLE 1

CRYSTALLITE SIZE OF γ-FeOOH FROM X-RAY DIFFRACTION PROFILES

Reflection	*Preparation No.*			
	1	*2*	*3*	*4*
002	—	—	210 Å	80 Å
020	780 Å	840 Å	80 Å	30 Å
040	700 Å	300 Å	—	—
080	680 Å	460 Å	170 Å	—
011	890 Å	680 Å	470 Å	—
022	900 Å	570 Å	200 Å	—
120	—	—	—	80 Å

Table 1 gives the crystallite sizes where available from x-ray reflection profiles. Figure 2 represents the crystallite size distribution, as determined from electron micrographs, for the length of needles of preparation 1. It is log normal. The needle length distribution of sample 2 was similar, while the needle breadth distributions were Gaussian. Sample 3 and 4 were too finely divided for proper counting.

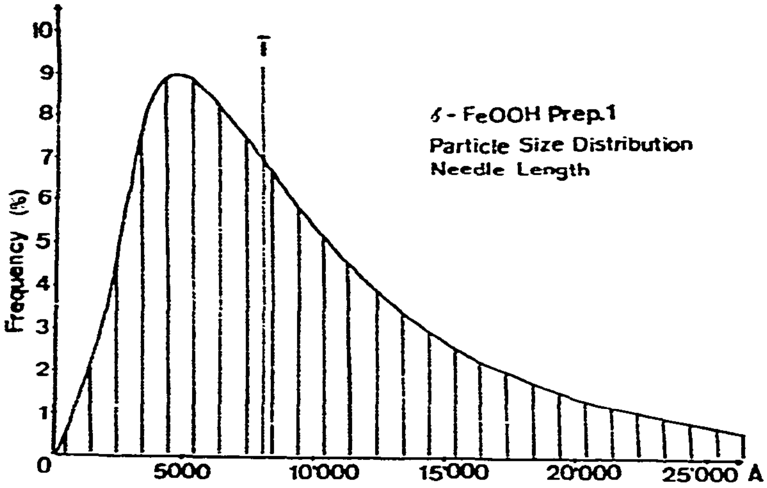

Fig. 2. Typical particle size distribution (example). Preparation 1, needle length.

The dimensions of the γ-FeOOH crystals are shown in Table 2. Samples 3 and 4 are not included, as their crystal dimensions were only estimated. No. 3 had approximately 1000 × 200 × 40 Å and No. 4 2000 × 400 × 80 Å dimensions. The BET surface of all samples is given in Table 3, the water content in Table 4.

TABLE 2

CRYSTALLITE SIZE OF γ-FeOOH FROM ELECTRON MICROGRAPHS

	Preparation No.		*Distribution*
	1	*2*	
Length	8130 Å, $\delta = 2.17$	6770 Å, $\delta = 2.23$	log normal
Breadth	1700 Å ± 600 Å	1100 Å ± 460 Å	Gaussian
Estimated thickness	340 Å	220 Å	—

TABLE 3

BET SURFACE OF γ-FeOOH

	Preparation No.			
	1	*2*	*3*	*4*
BET surface ($m^2\ g^{-1}$)	14.0	18.4	119.4	91.5

TABLE 4

TOTAL H_2O AND ADSORBED H_2O OF γ-FeOOH

	Preparation No.			
	1	*2*	*3*	*4*
Found %	12.7	12.5	16.7	16.6
Difference to 10,14% (theoretical) in %	2.6	2.4	6.6	6.5

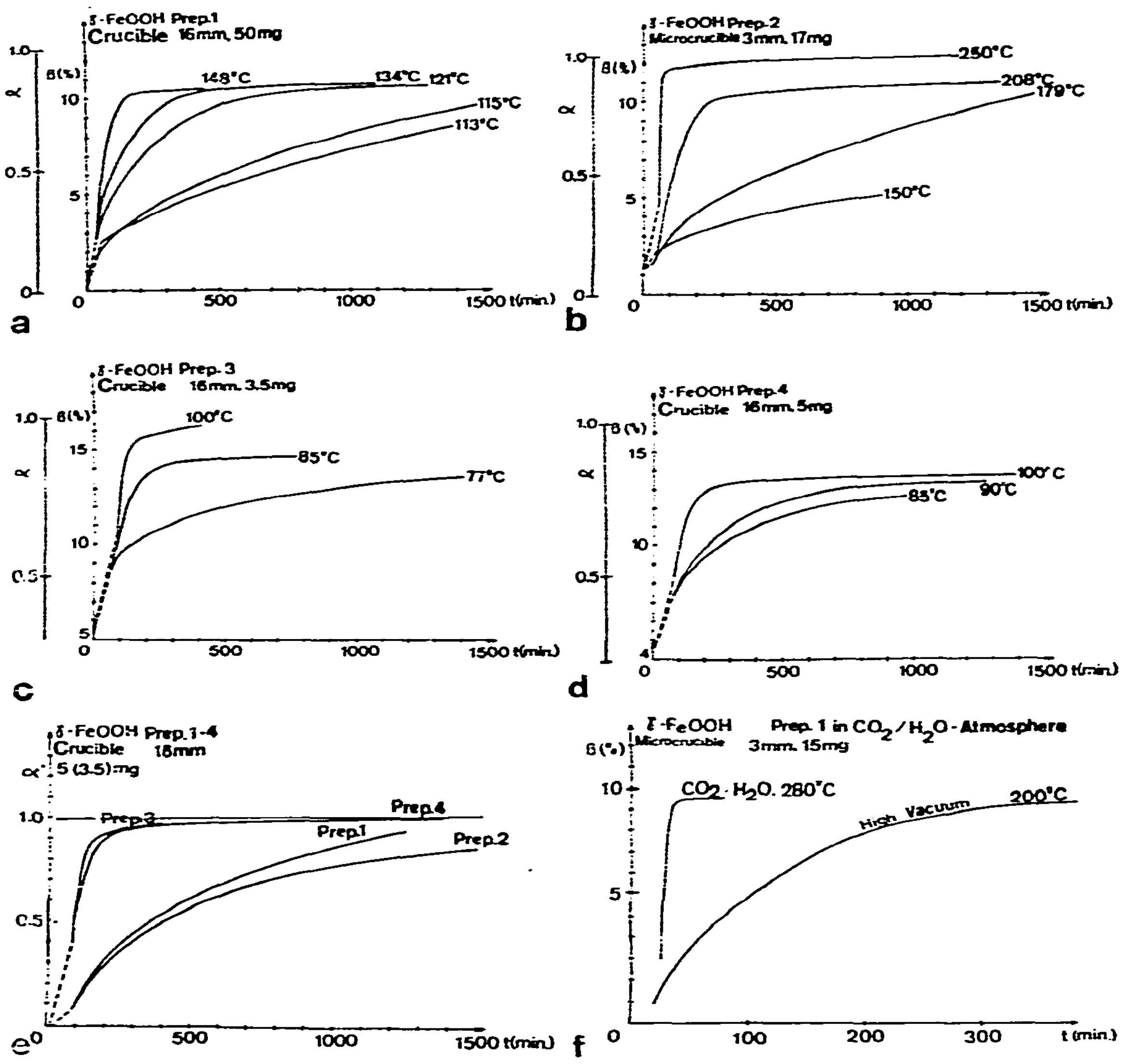

Fig. 3 Isothermal decomposition at various temperatures. (a) Preparation 1 decomposed in vacuo. (b) Preparation 2 decomposed in vacuo. (c) Preparation 3 decomposed in vacuo. (d) Preparation 4 decomposed in vacuo. (e) Influence of crystallite size on decomposition at 100 °C in vacuo. (f) Influence of atmosphere (water vapour pressure) on isothermal decomposition of preparation 1.

2. *Isothermal decomposition*

2.1 Decomposition in vacuo. Decomposition curves in vacuo of samples No. 1–4 are of similar shape. The reaction starts very fast, slows down within about 0.5–5 h (after having reached isothermal conditions) and ends sluggishly (Fig. 3). It should be noted, however, that no one set is actually identical to any of the others. In some instances, whole sets have been repeated to get more data. The measurements could be improved (in reproducibility) with larger samples: under such conditions, however, the decomposition water is not removed fast enough even under 10^{-5} torr, and a water vapour pressure builds up thus increasing the reaction rate as will be shown later. This being most undesirable, we were forced to accept the compromise of smaller samples and poorer reproducibility. The sample thickness could not be brought below 0.5 mm*.

As we shall see from x-ray evidence a H_2O atmosphere increases the reaction rate. Nevertheless Fig. 3b which represents a compressed sample shows a decrease in the reaction rate. The explanation is that in fact the reaction is faster but the desorption of the water is much slower, the balance pan then erroneously giving too high a sample weight (including H_2O) thus leading to the false conclusion of a slower reaction while it is actually enhanced.

This, like some other phenomena, underlines the importance of checking TG results by independent measurements.

As expected sample 3 with the smallest crystallite size (highest specific surface) decomposes faster than all three others, as can be seen from Fig. 3e which shows the TG curves at 100°C for all four samples. α' is the decomposed fraction:

$$\alpha'(t) = \frac{y(t)-x}{y_0-x}$$

where: $y(t)$ = weight loss after time t; x = weight loss during evacuation; y_0 = weight loss attained at constant weight.

2.2 Decomposition in H_2O atmosphere. A set of isothermal decomposition curves under water vapour would have been desirable; but for reasons of time, only one run at 280°C could be undertaken and may be shown together with a vacuum experiment at 200°C (Fig. 3f). p_{H_2O} was 646 torr; the carrier gas was CO_2. Although the two curves in Fig. 3f are not directly comparable, it is obvious that H_2O enhances the decomposition. This is backed by x-ray evidence. The x-ray identification of the end product of Fig. 3f proves that not only is the reaction faster but also α-Fe_2O_3 has nucleated (Fig. 4).

3. *Reduced time plots*

Results as shown above in real time may be approximated by least square methods to a very high degree of accuracy. This is, in our view, misleading, as such

---

*The layer thickness in Fig. 8 is a calculated value from sample weight and crucible diameter and may therefore be below 0.5 mm.

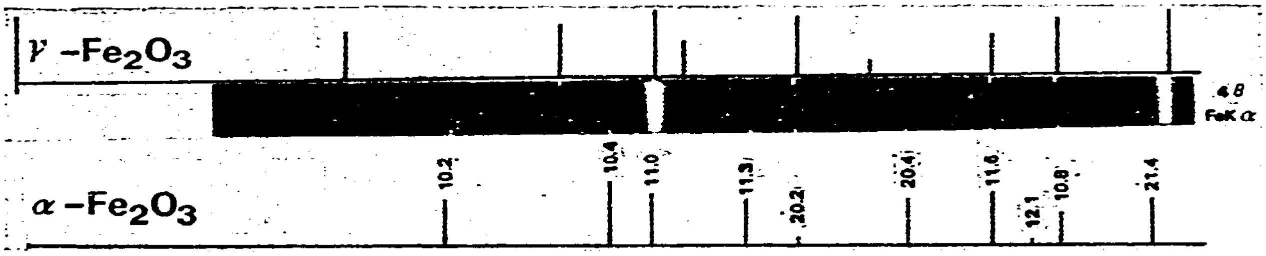

Fig. 4. X-ray powder pattern of product from isothermal run under water vapour (cf. Fig. 3f).

TABLE 5

Symbol	*Mathematical expression*	*Denomination*
D_1	$\alpha^2 = kt$	One-dimensional diffusion; parabolic law; Wagner's law
D_2	$(1-\alpha)\ln(1-\alpha)+\alpha = kt$	Two-dimensional diffusion for cylinder
D_3	$[1-(1-\alpha^{\frac{1}{3}}]^2 = kt$	Three-dimensional diffusion for sphere
D_4	$(1-\frac{2}{3}\alpha)-(1-\alpha)^{\frac{2}{3}} = kt$	Three-dimensional diffusion for sphere
F_1	$-\ln(1-\alpha) = kt$	Random nucleation; first order law
A_2	$\sqrt{-\ln(1-\alpha) = kt}$	Random nucleation; (Avrami equation)
A_3	$\sqrt[3]{-\ln(1-\alpha) = kt}$	Random nucleation (Avrami–Erofeyev equation)
R_2	$1-(1-\alpha)^{\frac{1}{2}} = kt$	Phase boundary controlled reaction for disc
R_3	$(1-(1-\alpha)^{\frac{1}{3}} = kt$	Phase boundary controlled reaction for sphere

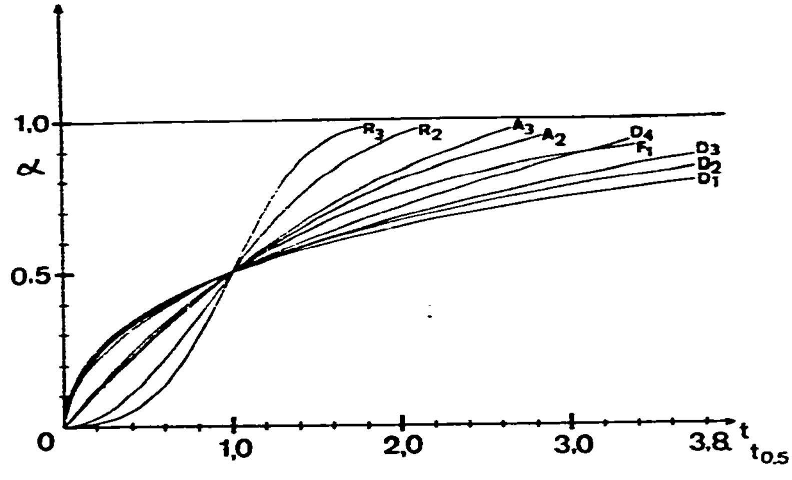

Fig. 5. Reduced time representation of time laws from Table 5.

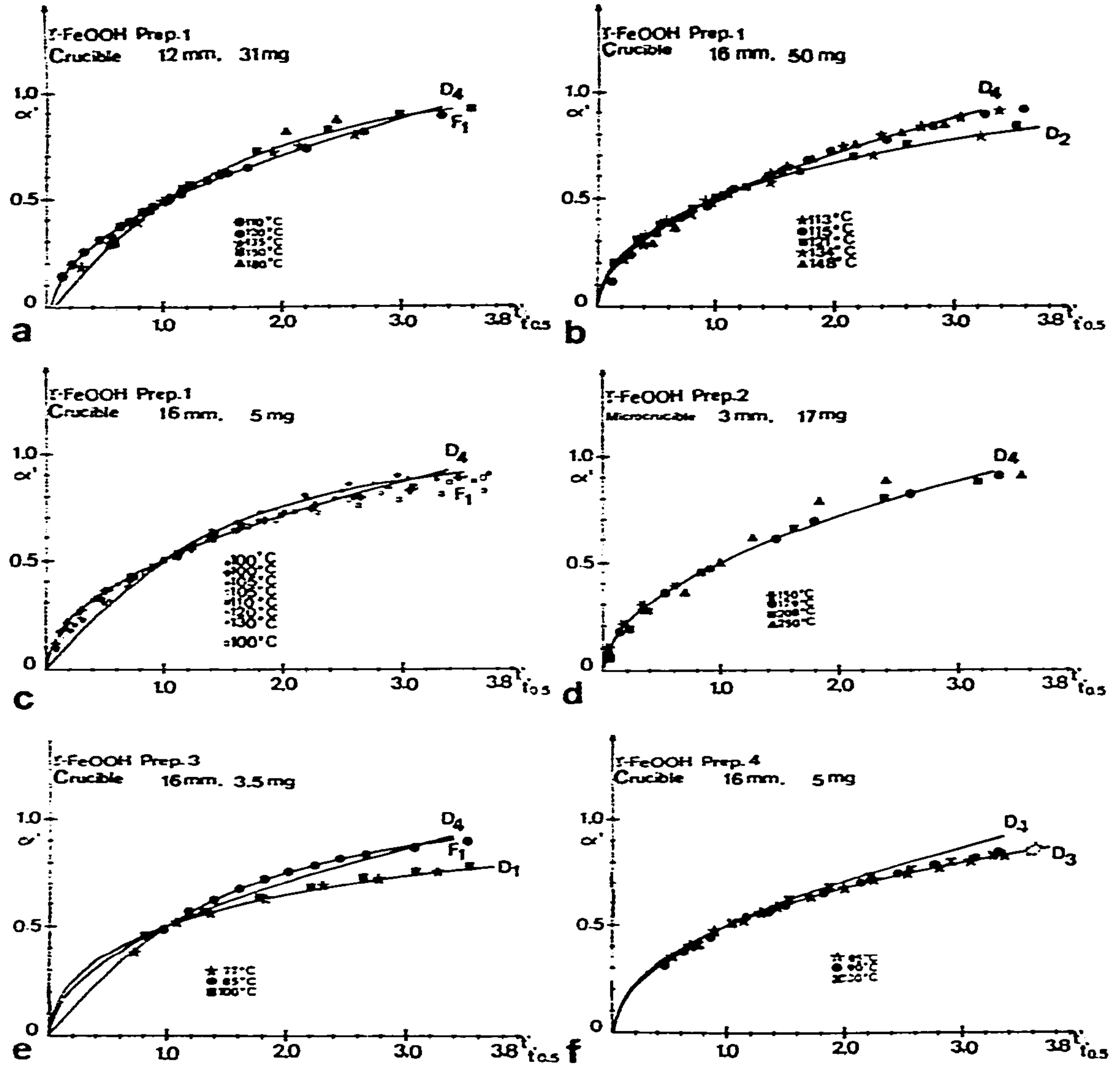

Fig. 6. Isothermal dehydration of 4 samples of γ-FeOOH at various temperatures in vacuo. Reduced time representation. The drawn out functions are those of Fig. 5. (a) Preparation 1, crucible 12 mm ⌀, 31 mg. (b) Preparation 1, crucible 16 mm ⌀, 50 mg. (c) Preparation 1, crucible 16 mm ⌀, 5 mg. (d) Preparation 2, crucible 3 mm ⌀, 17 mg. (e) Preparation 3, crucible 16 mm ⌀, 3.5 mg. (f) Preparation 4, crucible 16 mm ⌀, 5 mg.

presentations can eo ipso not be compared with each other. The way to overcome this difficulty has been shown, amongst others, by Delmon[7] in using a reduced time plot. The ordinate shows the decomposed fraction (from 0 to 1) after correction for adsorbed water, and the abscissa is drawn out in multiples of the half-time ($t/t_{1/2}$). Under such conditions the most important time laws as listed in Table 5 take the form of Fig. 5 and are either sigmoid or monotonous functions. It is crucial at this point to realize that only this reduction on both coordinates is capable to visualize the actual error range of such measurements. It can be quite difficult to extrapolate back to the start of the reaction from the point where isothermal conditions are attained, etc.

In Fig. 6 the results of a series of runs with various preparations are shown as examples out of a larger collection of data. For comparison some of the functions of Table 5 are drawn out. We would also like to draw the attention to the fact that particle size distributions can change the shape of fractional decomposition curves considerably. It is often overlooked that this factor usually is much more important than the reaction mechanism itself. Gallagher[8] has investigated the influence of a log normal distribution of spherical particles on a mechanism with one-dimensional diffusion. The broader the distribution, the faster is the starting period of the reaction up to 50%, and the more sluggishly ends the reaction. Figure 7 shows the fractional decomposition as a function of

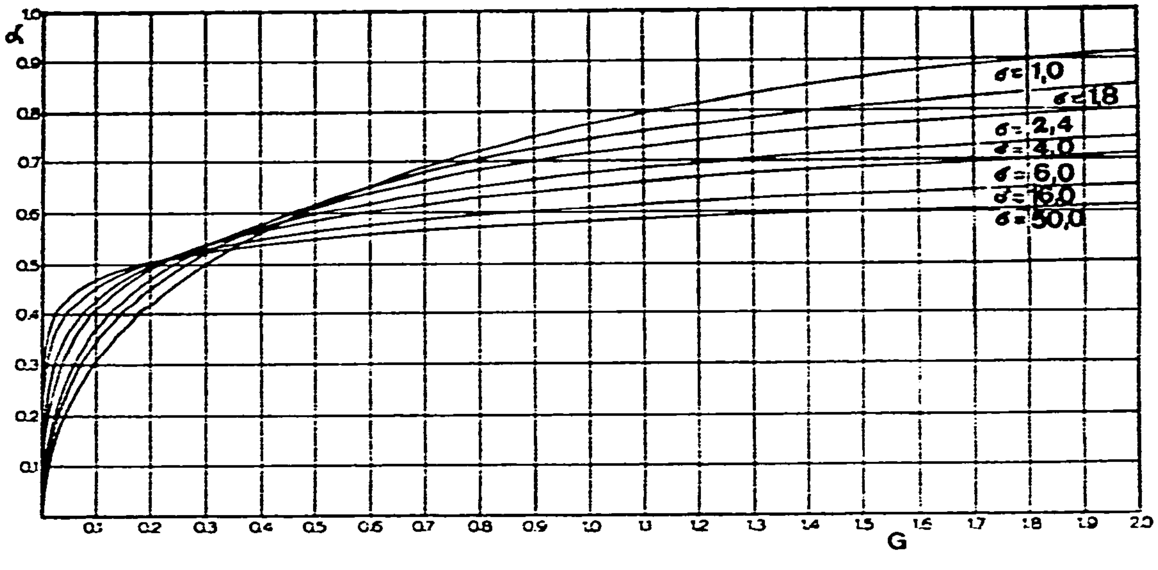

Fig. 7. Influence of particle size distribution on a particular reaction (D1)[8].

$$G = \frac{\Pi^2 \cdot D \cdot t}{a^2}$$

where D is the diffusion coefficient, t the time, and a the geometrical mean of the sphere radius (from the volume distribution).

4. *Unisothermal decomposition*

Preliminary experiments with samples from 2 to 100 mg of preparation 1 showed the influence of the filling height in the crucible on the decomposition rate

(Fig. 8). Below a minimal and above a certain height the influence becomes less obvious. Within the range shown the decomposition again was apparently slower with larger samples than with small samples. This collides with x-ray evidence shown in Fig. 4.

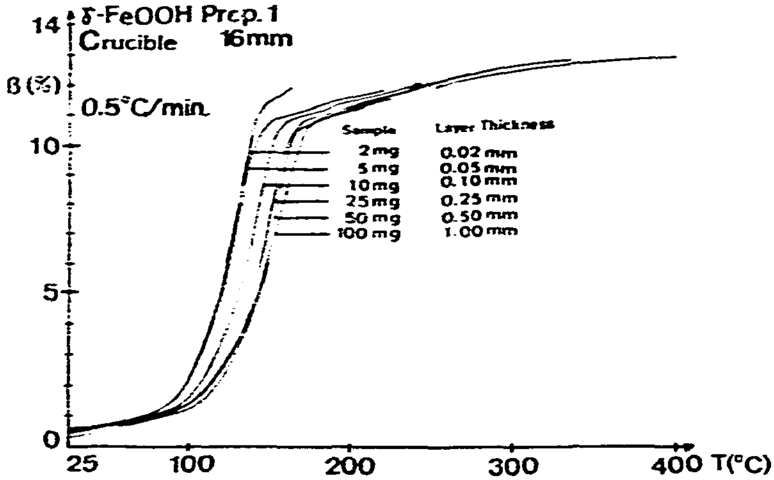

Fig. 8. Influence of filling height on decomposition of γ-FeOOH.

Unisothermal runs were undertaken in order to apply Šatava's method to determine the activation energy[9] (see below). Figure 9 shows typical unisothermal decomposition curves. The form of such curves turned out to be heavily influenced by the heating rate. High heating rates expand the range of temperature within which the reaction is accomplished. This is undoubtedly an advantage for the subsequent evaluation. On the other hand the sample (a usually poor heat conductor) will at

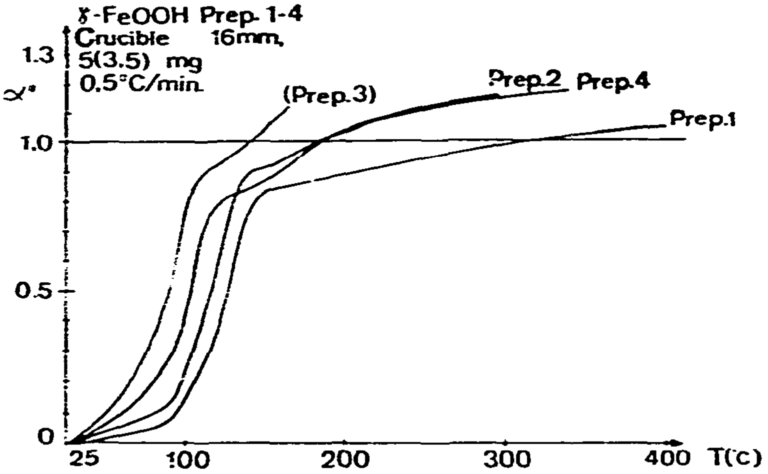

Fig. 9. Unisothermal dehydration of γ-FeOOH (sample curves).

high heating rates no longer provide a smooth reaction. Under our conditions already a heating rate of 2°C min^{-1} produces a non-uniform release of water which is most undesirable as the water vapour pressure within the sample then builds up to considerable values and influences the reaction. Therefore all unisothermal experiments were done at the lowest possible rate of 0.5°C min^{-1}.

The four preparations, decomposed under identical conditions, may be compared here directly: The thermal stability decreases, as expected, with the specific surface. Up to about 80% decomposition all curves are very similar and only their location along the temperature axis varies. In other words the mechanism remains the same and only the pre-exponential factor is affected. The curves show, furthermore, that the weight loss due to dehydration approaches with increasing temperature more and more the region where the subsequent transformation to Fe_3O_4 under loss of oxygen begins. The three reactions

$$2\gamma\text{-FeOOH} \longrightarrow \gamma\text{-Fe}_2\text{O}_3 + \text{H}_2\text{O}$$

$$\gamma\text{-Fe}_2\text{O}_3 \longrightarrow \alpha\text{-Fe}_2\text{O}_3$$

$$3\alpha\text{-Fe}_2\text{O}_3 \longrightarrow 2\text{Fe}_3\text{O}_4 + 1/2\ \text{O}_2$$

can thus not be clearly separated under the circumstances, nor is it possible to detect a plateau corresponding to desorption of physisorbed water before the dehydration starts.

5. *Activation energy from isothermal data*

In Fig. 10 the function $-\log d\alpha'/dt$ is plotted versus $1/T$, according to Wiedemann's method[10]. The slope yields the figures of Table 6. All activation energies are close to $\approx$ 29.5 kcal and deviations do not show any significant relation to the sample history nor to reactions conditions. The pre-exponential factor, however, is clearly

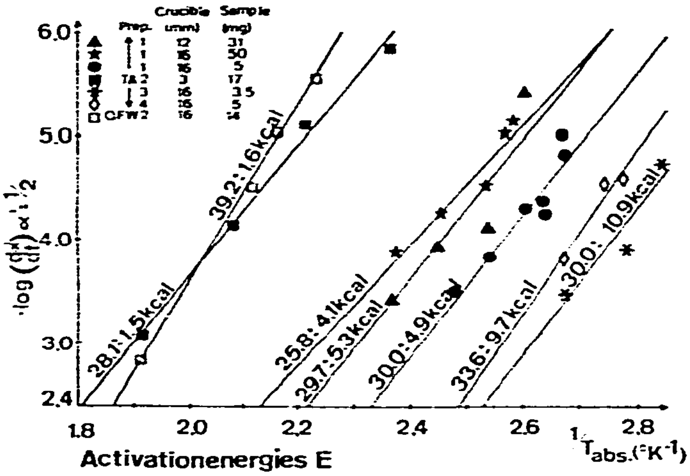

Fig. 10. Activation energies from various data collections.

TABLE 6

ACTIVATION ENERGIES FROM ISOTHERMAL DATA

Preparation No.	*Crucible diameter (mm)*	*Sample (mg)*	*Activation energy (kcal mol^{-1})*	*Pre-exponential factor*
1	12	31	29.7 ± 5.3	$9.5 \cdot 10^{11}$
1	16	50	25.8 ± 4.1	$4.1 \cdot 10^{9}$
1	16	5	30.0 ± 4.9	$7.0 \cdot 10^{12}$
2	Microcrucible	17	28.1 ± 1.5	$4.2 \cdot 10^{8}$
3	16	3.5	30.0 ± 10.9	1.6 ± 10^{14}
4	16	5	33.6 ± 9.7	$8.1 \cdot 10^{15}$

higher for the finely divided samples 3 and 4 as compared to 1 and 2. It might be added here that further experiments with higher filled crucible (higher sample thickness) produced lower pre-exponential factors.

6. *Activation energies from unisothermal data*

Šatava's[3] method to determine graphically from unisothermal data the activation energy has the advantage that it takes into account the entire reaction while in methods using isothermal data the beginning of the reaction usually must be discarded as it will be part of the heating period. It has the grave disadvantage that the reaction mechanism must be known for proper evaluation*.

If we assume the time law D4 of Table 5 to be the best approximation for our reduced time isothermal data, and if we plot Šatava's function log $g(\alpha)$ versus T, we get Fig. 11 and Table 7. In the latter the isothermally obtained data are included for comparison. The results are well within the experimental errors of the different methods and thus in satisfactory agreement.

7. *X-ray diffraction*

The following particle sizes of γ-Fe_2O_3, produced in the thermobalance in vacuo at 150°C (preparation 1) and in the furnace in vacuo at 200°C (preparation 3 and 4) were found (Table 8). All values are well within the limits of experimental error which has been estimated by Bartram[11] to be ± 1 Å (or $\pm 1\%$) for crystallite sizes around 82 Å but which, according to our own experience, is much higher. It should be noted here that the reflection 440 at $2\theta = 82°$ (FeK_α) has been indexed 525 by Schrader[12].

According to Table 8 the γ-FeOOH crystals break into tiny, more or less equal crystallites, irrespective of the initial crystallite size. This is in accord with x-ray powder diffraction evidence (Fig. 12) although on the whole this seems to be highly suspicious for a reaction assumed to be topotactical.

---

*In Šatava's publication this is not a priori necessary. The application in our case showed, however, that it may be very difficult to operate without known formal time law.

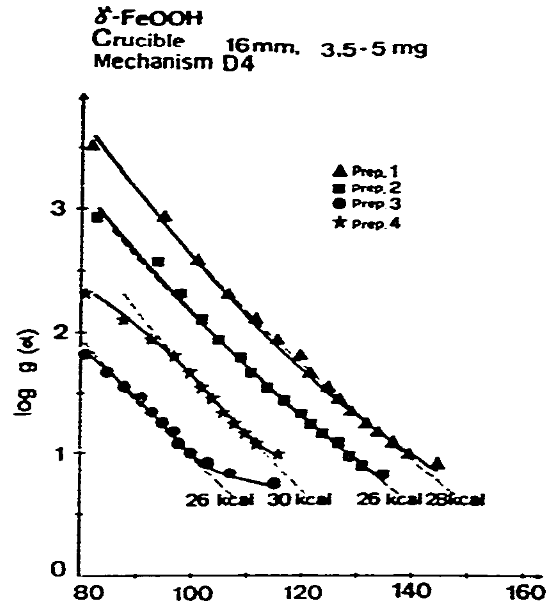

Fig. 11. Activation energies determined after Šatava[9].

TABLE 7

ACTIVATION ENERGIES FROM UNISOTHERMAL DATA

Preparation No.	*Crucible diameter (mm)*	*Sample (mg)*	*Activation energy*[a] *(kcal mol^{-1})*	*Pre-exponential factor*[a]
1	16	5	28±2 (30.0±4.9)	$5.9 \cdot 10^{10}$ ($7.0 \cdot 10^{12}$)
1	16	52	30±2 (25.8±4.1)	$9.6 \cdot 10^{10}$ ($4.1 \cdot 10^{9}$)
2	16	5	26±2	$1.1 \cdot 10^{10}$
2	16	52	28±2	$1.2 \cdot 10^{10}$
3	16	3.5	26±2 (30.0±10.9)	$1.6 \cdot 10^{11}$ ($1.6 \cdot 10^{14}$)
3	16	42	20±2	$4.5 \cdot 10^{6}$
4	16	5	30±2 (33.6±9.7)	$9.2 \cdot 10^{12}$ ($8.1 \cdot 10^{15}$)
4	16	52	20±2	$1.6 \cdot 10^{6}$

[a] In brackets figures from Table 6 for comparison.

TABLE 8

PARTICLE SIZE OF γ-Fe_2O_3 FROM X-RAY PROFILE ANALYSIS

	Crystallite size from profile of reflection			
γ-Fe_2O_3	220	113	400	440
From preparation 1	27 Å	32 Å	72 Å	71 Å
From preparation 3	20 Å	29 Å	42 Å	43 Å
From preparation 4	17 Å	27 Å	34 Å	35 Å

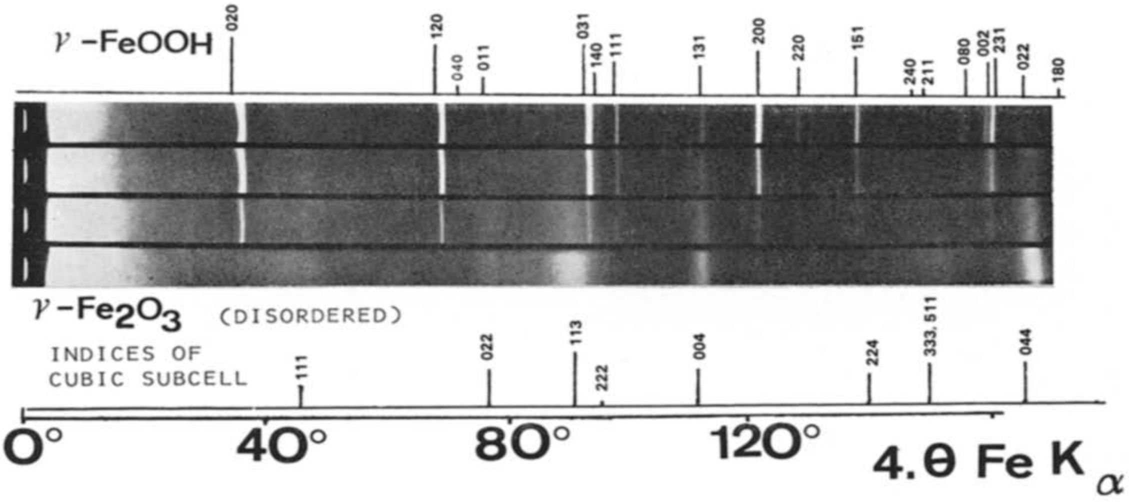

Fig. 12. Guinier patterns of four samples of partly decomposed γ-FeOOH (preparation 1) produced in vacuo at 115 °C. From above: Fractional decomposition ca. 25, 50, 74 and 83%.

8. *BET surface*

In order to check the mentioned, astonishingly low crystallite size, BET measurements of the specific surface made on the Cahn balance directly after decomposition (without breaking the vacuum) as well as those from samples decomposed in vacuo in a tube furnace may be compared in Table 9. The data from BET surface determinations have two features worthwile pointing out. First, the particle sizes differ by a factor no less than two, depending on whether or not the samples have been in contact with room air (i.e., moisture). Secondly, there is a fairly good agreement between values of column 1 and 3; i.e., whenever the BET measurement has been done without breaking the vacuum, the resulting particle size is within an order of magnitude comparable to the x-ray crystallite size.

TABLE 9

PARTICLE SIZE (Å) (CUBE EDGE) OF γ-Fe_2O_3. FROM BET MEASUREMENTS

	History (decomposition at 150–200 °C)		
	Produced on Cahn balance without breaking vacuum	*Produced in tube furnace in vacuo, transferred to Cahn balance via air*	*Produced in tube furnace, from x-ray line profile, for comparison*
γ-Fe_2O_3			
From preparation 1	87	167	72
From preparation 2	97	—	—
From preparation 3	69	88	42
From preparation 4	81	122	35

It may be interesting to note that a decomposition product from preparation 2, decomposed at 440 °C on the Cahn balance, and measured without ever having been in contact with air, gave a specific surface of only 23.8 $m^2 g^{-1}$. The substance consisted according to x-ray diffraction of α-Fe_2O_3 and the particle size derived from this surface is 480 Å (cube edge or equivalent sphere diameter). This clearly indicates *that the subsequent transition of γ-Fe_2O_3 into α-Fe_2O_3* is connected with sintering effects. In other words, two entirely different methods give identical and conclusive evidence of a total disruption of the initial crystals of γ-FeOOH into tiny cubes of γ-Fe_2O_3. This of course eliminates at least for the final stage of the reaction all phase boundary controlled mechanisms, as the rate determining step in this stage is to push the reaction water out of the pore system of the extremely finely divided end product.

9. *Electron microscopy*

9.1 Electron diffraction. The evidence accumulated so far has only in part been satisfactory. It therefore seemed desirable to look directly at (and into) the γ-FeOOH crystals at various stages of their decomposition. While the initial γ-FeOOH showed the usual Bragg fringe contrast this was not the case in the uniformly grey final γ-Fe_2O_3. Yet the size and shape of the crystals did not alter and the selected area electron diffraction of single crystal changed gradually from that of γ-FeOOH (b^* c^* zone) into that of apparent γ-Fe_2O_3 single crystals. The orientation of the latter was always that described by previous authors, one axis being [110] in the pseudocubic notation and the other [001] as shown in Fig. 13.

We shall deal with the disappearing Bragg fringes in Section 9.2 and look first into the diffractions. According to our experience, reflections in electron diffraction are sharp if more than about 20 identity periods (unit cells) scatter coherently. Whenever between about 5 and 20 periods contribute to a reflection, it will be broadened and can be treated according to the Scherrer equation. Less than about 5 coherently scattering periods do not produce a reflection. The appearance of such an electron diffraction will be that of an "amorphous" substance.

As we do not find tetragonal supercell reflections in any of our γ-Fe_2O_3 diffractions, and as the other reflections are considerably broadened, we may assume qualitatively that the crystallite size of our γ-Fe_2O_3 produced in vacuo is less than 5 identity periods of the supercell but more than 5 periods of the pseudocubic subcell, i.e., 40–120 Å. This is in excellent agreement with figures in Table 9.

γ-Fe_2O_3 from preparation 2 produced in 1 h at 320 °C under atmospheric pressure shows less broadened reflections in its electron diffractions, not presented here for the sake of brevity. This confirms the already outlined importance of the H_2O partial pressure on the reaction. Figure 14 underlines this point by showing two products, the history of which differs only in the water vapour pressure. In vacuo perfectly pseudomorphous γ-Fe_2O_3 is obtained while under atmospheric pressure but otherwise similar conditions α-Fe_2O_3 with beginning sintering effects occur. The products were checked by x-ray diffraction. Thus the water vapour pressure has allowed nucleation of another phase than that occurring in vacuo. This underlines one of our aims, namely to show that kinetics and even the mechanism of decomposition reactions with H_2O evolution are subject to the influence of the H_2O partial pressure to such an extent that any mechanisms derived only from formal measure-

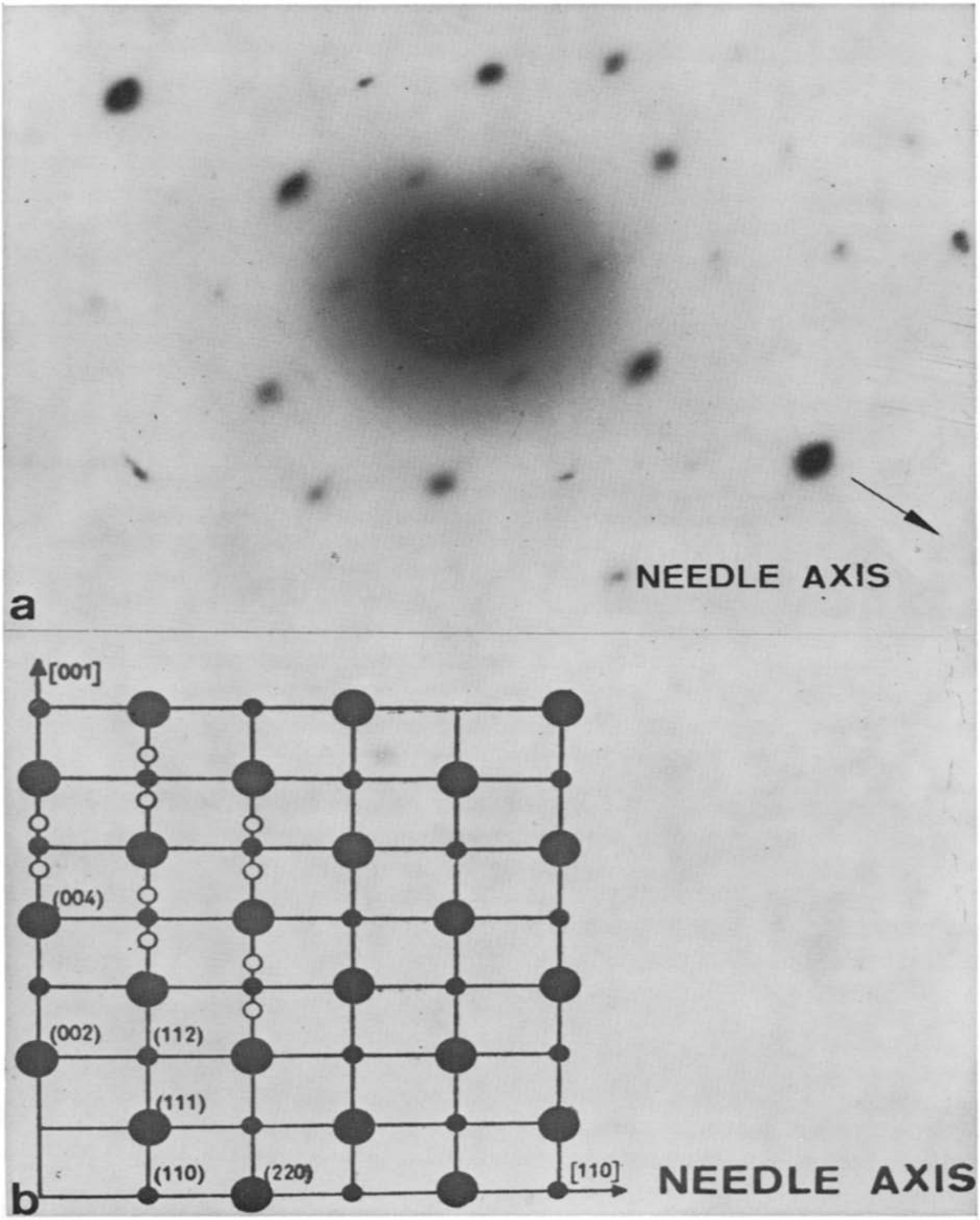

Fig. 13. (a) Selected area electron diffraction of γ-Fe_2O_3 (preparation 2; 1 h, 400 °C, 10^{-4} torr). (b) Idealized indexed diffraction with super cell reflections. The indices refer to the cubic subcell of γ-Fe_2O_3.

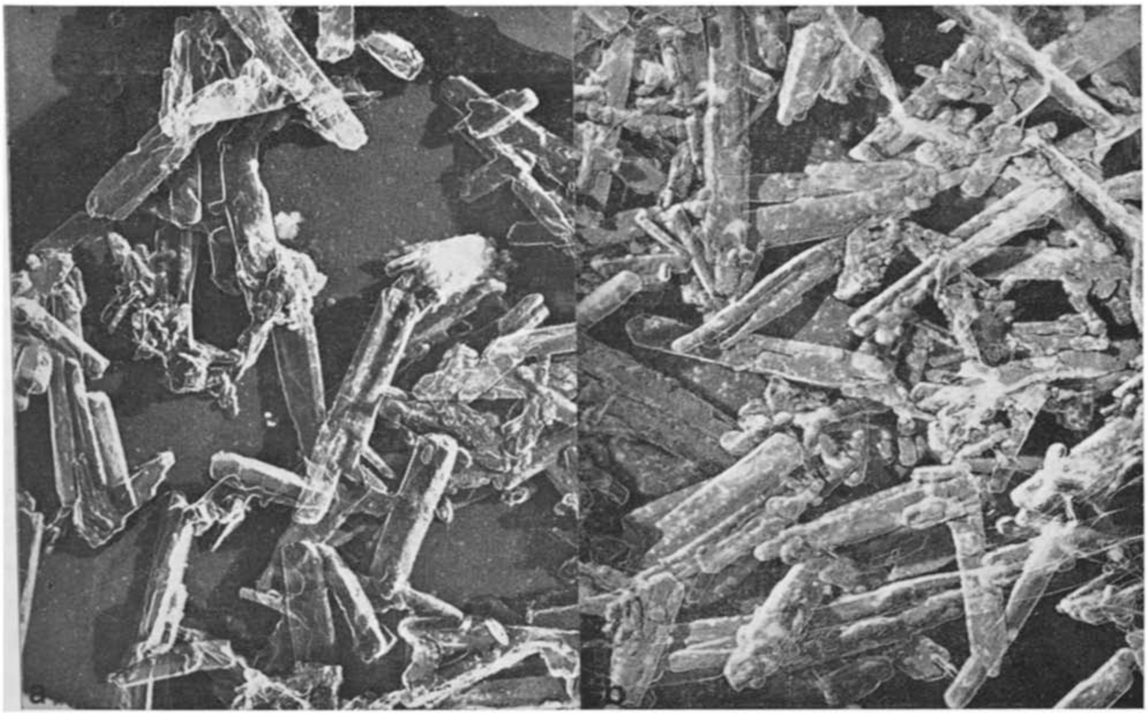

Fig. 14. Electron micrographs of products from γ-FeOOH (preparation 2). (a) In vacuo, 400 °C, 1 h: γ-Fe_2O_3 (30'000×). (b) Atmospheric pressure, 380 °C, 1 h: α-Fe_2O_3. Mind the beginning crystallite growth (30'000×).

ments must remain highly dubious. Decomposition of hydroxides, etc. yielding reaction water must be studied in vacuo to produce meaningful kinetics.

9.2 Texture of γ-Fe_2O_3. As mentioned before, the initial Bragg fringe contrast of the γ-FeOOH crystal vanishes with proceeding reaction. For interpretation of this phenomenon it is necessary to recall what the presence or absence of Bragg contours actually means.

In very thin crystals, the reciprocal lattice points will be elongated to spikes vertically to the platelet zone. As the Ewald sphere is, due to the very short wavelength of the electron beam, so large that a tangent plane may replace it, there will virtually always be a cut of this tangent plane through some reciprocal lattice spikes. In other words, the Bragg condition of diffraction is always fulfilled and a diffraction pattern will be produced by the entire crystal. The real crystal differs from this situation only in that it is, as a rule, slightly bent, which means that the Bragg condition is not equally well fulfilled throughout the crystal. Where it is fulfilled, the diffracted beam will be deflected at an angle prohibiting this beam to pass through the objective diaphragm. That is to say this part of the initial beam does not contribute to the final image and there will, thus, be a dark region in this image showing where the missing part of the beam (i.e., the diffracted beam of one particular Bragg condition, defined by the hkl of the according lattice plane family) originally came from. By shifting the objective diaphragm from the primary beam to the said reflection, a dark field picture in the light of this particular beam, or reflection, will be obtained. In this dark field picture the region which before, in the normal position of the objective diaphragm, has been dark against bright background, will show bright against dark background. By switching the image conditions to diffraction, the reflection can be identified. Hence, it is possible to attribute each dark zone in a picture of γ-FeOOH to a particular family of planes named hkl which originates there. Such regions are called Bragg fringes, or Bragg contours, or extinction contours, etc. In many cases it is possible, with the present state of the art, to make directly visible these lattice planes.

A closer investigation of partly decomposed γ-FeOOH crystals, now, reveals at higher magnification some surprising and highly characteristic features (Fig. 15). Some parts of the crystal exhibit the said Bragg fringes, while other parts do not. Along the needle axis another contrast phenomenon is visible, in the form of strings of aligned "particles" of the size of about 70 Å. These can only be the crystallites of γ-Fe_2O_3 which are forming in the γ-FeOOH matrix crystal. Where Bragg fringes occur, the γ-FeOOH is still coherently scattering, and where these γ-Fe_2O_3 crystallite strings intrude, a sharp contrast indicates the interface. By depicting a γ-FeOOH

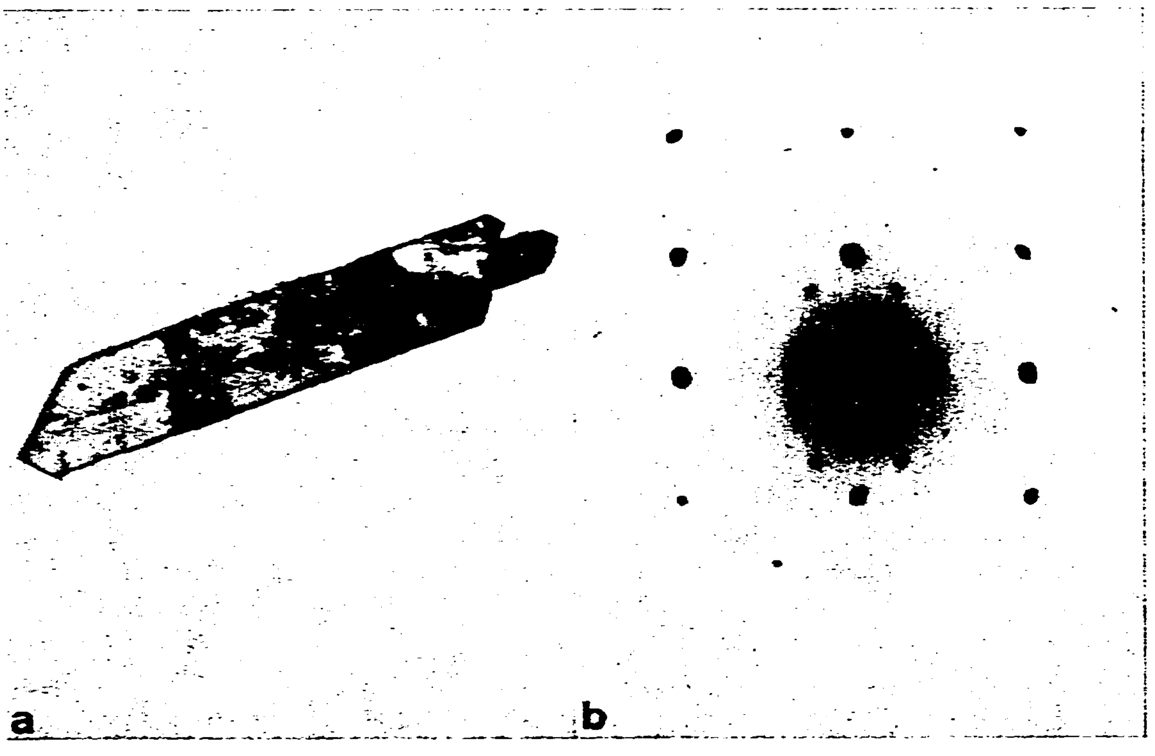

Fig. 15. (a) Partly decomposed crystal of γ-FeOOH (115°C, 10^{-5} torr, $\alpha \approx 25\%$) (75'000×). (b) Selected area electron diffraction of the above crystal. This is a superposition of the γ-FeOOH pattern and the (weak) γ-Fe_2O_3 reflections.

reflection and imaging the crystal in the dark field mode we can, according to the above explanation, produce a dark field picture of the undecomposed γ-FeOOH while an analogous dark field picture in the light of an appropriately selected γ-Fe_2O_3 reflection shows the decomposed parts, i.e. the γ-Fe_2O_3, within the matrix crystal.

From a series of such pictures we conclude that the γ-Fe_2O_3 in Fig. 15 is not a single crystal but a polycrystalline aggregate so perfectly orientated that its texture pattern could be mistaken for a single crystal electron diffraction. Secondly the pictures indicate that the more the reaction proceeds, the smaller are the coherently scattering regions in a crystal (i.e. γ-FeOOH), and the larger become the regions of non-coherently scattering γ-Fe_2O_3 crystallites within the initial platelet.

In the beginning stage of the reaction, γ-Fe_2O_3 forms predominantly at edges, cracks, and other defects even in the interior of a crystal. Later on, these "nuclei" of 70 Å size give rise to formation of further γ-Fe_2O_3 crystallites of the same size, and this proceeds almost exclusively along the needle axis direction. Towards the end of the reaction the growth of a decomposed region proceeds also sideways and very fast. In the end the mentioned pseudomorphous, perfectly oriented aggregation of γ-Fe_2O_3 crystallites fills out the initial space of the γ-FeOOH crystal. The sharp contrast present in the early stage of the reaction fades away and in the end a uniformly grey platelet is visible.

As we were interested to know whether or not these γ-Fe_2O_3 crystallites in the aggregation could grow to a larger size in an appropriately slow decomposition, we ran an unisothermal one-month decomposition (heating rate such that the weight loss remained 0.3 mg per day; from ambient temperature to 200°C, 10^{-5} torr). The attained fractional decomposition after one month was ca. 77% and the apparent particle size (from a BET surface of 87.9 $m^2\ g^{-1}$) about 130 Å. This apparent particle size and BET surface correspond entirely to the unfinished reaction; a second run with heating rate ca. 2°C min^{-1} and otherwise the same conditions has led to $\alpha \sim 0.91$ and a BET surface of 142.1 $m^2\ g^{-1}$ or particle size 83 Å. This proves that even extremely slow decomposition leads to polycrystalline γ-Fe_2O_3.

CONCLUSION

1. Lattice transformation

The electron micrographs show that the γ-FeOOH crystals decompose—once the decomposition is under way—to γ-Fe_2O_3 of about 70 Å size; i.e. through the entire thickness of the crystal in one event. The γ-FeOOH lattice consists of corrugated layers of $(FeO_6]$ octahedra, separated from each other by fairly strong hydrogen bonds. (Fig. 16a). γ-Fe_2O_3, on the other hand, may be described in terms of a defect spinel, and thus consists of a framework of ccp $[FeO_6]$ octahedra, with edge and corner sharing.

The electron microscopical evidence leads to the following assumption: The γ-FeOOH layers collapse such that by more edge and corner sharing O^{2-} ions become available to form H_2O on the one hand and a ccp of O^{2-} on the other hand.

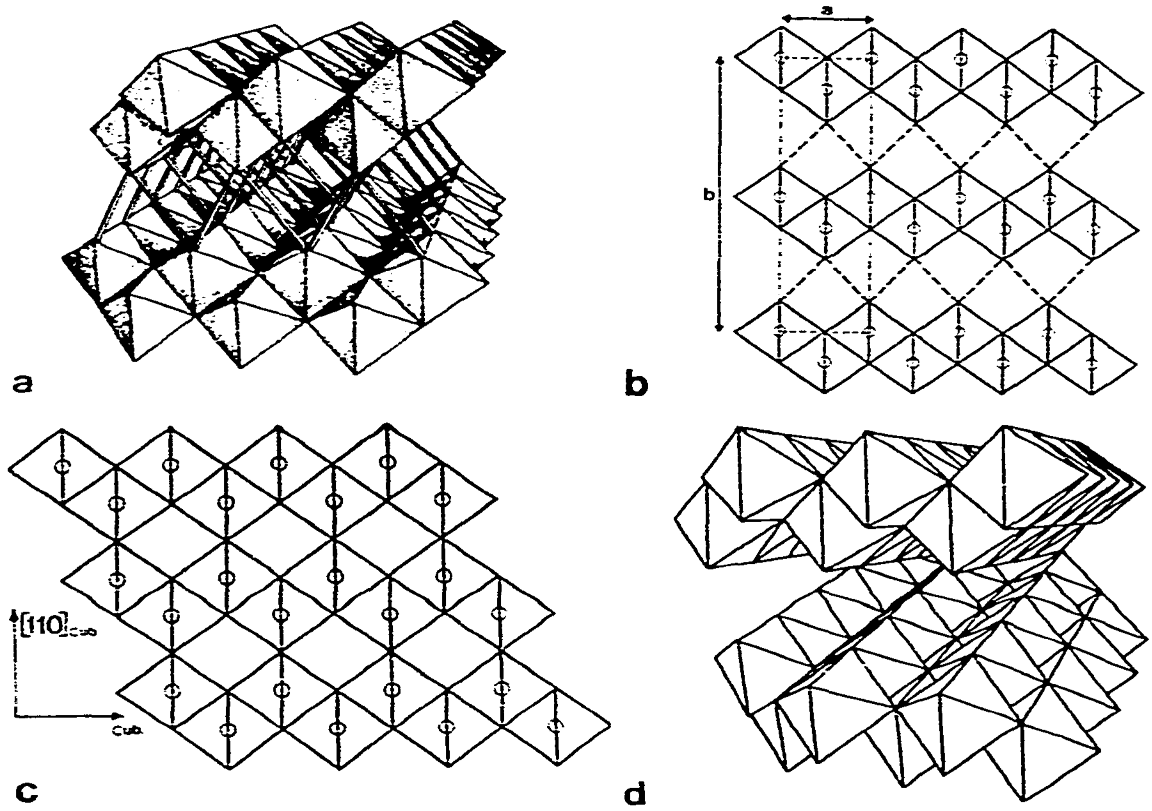

Fig. 16. (a) Lepidocrocite type (γ-FeOOH) with corrugated layers of [FeO_6] octahedra. (b) Projection of (a) along [001]. (c) Collapsed [FeO_6] layers forming a ccp and new (empty) octahedral sites. (d) Interface between intact γ-FeOOH (foreground) and collapsed layers forming γ-Fe_2O_3 (background).

This involves, however, an enormous lattice strain as shown in Fig. 16d. It is out of question that this lattice strain can be accomodated by the crystal, and the part of the γ-FeOOH decomposed must collapse, thus producing the crystallites of 70 Å size and the strong contrast phenomena shown in Fig. 15. It seems likely that the front and sides of such a γ-Fe_2O_3 crystallite act as nuclei for the proceeding reaction. If we accept this mechanism for the start of the reaction we also obtain immediately the answer to the otherwise unexplicable fact that by dehydration of γ-FeOOH fully ordered γ-Fe_2O_3 of the quality of that obtained by oxidation of Fe_3O_4 cannot be attained: Fe_3O_4 as a starting material provides the framework that allows diffusion of Fe^{3+} such that these can arrange themselves[3]. In our case, however, there is no chance that the Fe^{3+} ions find time in the short period of lattice disruption to get in place by a cooperative motion; and once the 70 Å crystallites of γ-Fe_2O_3 are formed, there is no longer a coherent matrix available for low temperature diffusion. The reaction water, furthermore, will partly be stuck at the interface between the γ-Fe_2O_3 crystallites. This again is all very well in accord with the extremely sluggish end stage of that reaction. The latter fact, taken for itself, might lead to the erroneous conclusion that

γ-Fe_2O_3 can never be produced without the presence of some H^+ (and accordingly Fe^{2+}, for the charge balance).

2. *Development of texture*

The reaction in question is directed by the initial lattice and hence leads to a highly oriented product, unless the water vapour pressure rises to a point allowing nucleation of α-Fe_2O_3. The reaction happens within the solid; it is topochemical. Since the movements of the ions involved follow two lattice dimensions of the initial γ-FeOOH, it may even be called topotactic, although we feel that we then stretch that concept to its very limits.

The reflections of the final γ-Fe_2O_3 are, at closer inspection, selectively broadened. This may be attributed to different crystallite dimensions in the according directions, or else to a disorder phenomenon. As we have already mentioned, the Fe^{3+} ions have scarcely time and occasion to arrange themselves; i.e. along a four-fold screw axis in the proper sequence ... □ □ Fe □ □ Fe ... (on the so-called "lithium sites" of the γ-Fe_2O_3 lattice). Under such conditions the 400 and 440 reflections of the cubic pseudocell are less affected than pyramid reflections, let alone the tetragonal supercell reflections which do not appear at all in our case.

In conclusion we may say that with respect to all these manifold ordering processes necessary to form fully crystalline γ-Fe_2O_3*, it is clearly impossible to go all along the reaction from γ-FeOOH single crystals to γ-Fe_2O_3 single crystals and the total disruption of the initial crystal into tiny bits of disordered γ-Fe_2O_3 is a necessity.

3. *Kinetics*

While the measured time law is, within the experimental error, compatible with the first order law (F1) as well as with diffusion controlled mechanisms (D1, D2, D3, D4), we can rule out all mechanisms leading to a sigmoid function. From this evidence alone it would be futile to speculate about the proper mechanism. The electron microscopical pictures, however, lead without any doubt to the conclusion that nucleation occurs all over the crystal at random. It is possible, or even probable, that the sluggish end part is directed by another law, namely by diffusion of H_2O molecules out of the polycrystalline γ-Fe_2O_3. This does not show in the decomposition curves, and the reduced time plots of diffusion controlled reactions are very similar to each other anyway.

We should like to point out, finally, that the electron micrographs give us the means to rule out the nomenclature "monocrystal with mosaic texture" as the new phase appears in places quite far apart from each other, and as new interfaces are formed

---

*Actually $Fe_{64}O_{96}$ or

$$\{Fe_{24}^{\mathrm{Tetrahedral}}\,[Fe_{36}^{\mathrm{Octahedral}}\,(Fe_{4}^{\mathrm{Li\text{-}sites}}\,\square_{8}^{\mathrm{Li\text{-}sites}})]\,O_{96}\}$$

ACKNOWLEDGEMENTS

Authors are grateful to Professor W. Feitknecht for valuable discussions and contributions, to Dr. K. J. Gallagher for help in sorting out kinetic problems and for providing Fig. 16a, and to Dr. H.-G. Wiedemann for experiments in the Laboratories of Mettler Instrumente AG. Authors are also indebted to Miss E. Ettinger for various contributions and to the Swiss National Fund for financial support.

REFERENCES

1 R. Giovanoli and R. Brütsch. *Chimia*, 28 (1974) 188.
2 W. Feitknecht, *Pure Appl. Chem.*, 9 (1964) 423.
3 K: J. Gallagher, W. Feitknecht and U. Mannweiler, *Nature*, 217 (1968) 1118.
4 J. D. Bernal, D. R. Dasgupta and A. L. Mackay, *Nature*, 180 (1957) 645.
5 D. R. Dasgupta, *Ind. J. Phys.*, 35 (1961) 401.
6 H. P. Klug and L. E. Alexander, *X-Ray Diffraction Procedures*, Wiley & Co., New York, 1954, p. 1959.
7 B. Delmon, *Rev. Inst. Franç. Pétr. & Ann. Combust. Liq.*, 18 (1963) 471.
8 K. J. Gallagher, in G. M. Schwab (Ed.), *Reactivity of Solids*, Proc. 5th I.S.R.S. Munich 1964, Elsevier, Amsterdam, 1965, p. 192.
9 V. Šatava and F. Škvára, *J. Amer. Ceram. Soc.*, 52 (1969) 591.
10 H. G. Wiedemann, A. V. Tets and H. P. Vaughan, presented 21st Feb. 1966, *Conference on Analytical Chemistry and Applied Spectroscopy, Pittsburgh*.
11 S. F. Bartram, in E. F. Kaelble (Ed.), *Handbook of X-Rays*, McGraw-Hill, New York, 1967, pp.17–19.
12 R. Schrader and G. Büttner, *Z. Anorg. Chem.*, 320 (1963) 205.